Effects of an inserted circular cylinder on a steady lid-driven rectangular cavity flow

IOP Conf. Series: Materials Science and Engineering **700** (2019) 012008 doi:10.1088/1757-899X/700/1/012008

Effects of an inserted circular cylinder on a steady lid-driven rectangular cavity flow

J Zhu, L E Holmedal and D Myrhaug

Dept. of Marine Technology, Norwegian University of Science and Technology, Trondheim, Norway

E-mail: jianxun.zhu@ntnu.no

Abstract. This paper provides numerical investigations of flow in a steady lid-driven cavity of depth to width ratio 1/3 containing a circular cylinder. The inner cylinder is treated using a direct-forcing immersed boundary method, and a project method is applied to solve the incompressible Navier-Stokes equations. Three different Reynolds numbers and positions of the cylinder are considered; for a lower Reynolds number, flow structures are weakly affected by the cylinder near the left wall while two clockwise vortices attached to the cylinder are formed as the cylinder moves rightwards; for a moderate Reynolds number, an anticlockwise bottom vortex is formed for the cylinder near the left wall, and it disappears as the cylinder is shifted rightwards; for the largest Reynolds number, two anti-clockwise vortices attached the cylinder are formed for the cylinder close to the left wall, and as the cylinder moves gradually closer to the left wall a bottom vortex is formed and disappears together with the clockwise vortex to the right side of the cylinder.

1. Introduction

Vortex structures, e.g. elongated primary vortices and corner vortices, within a steady lid-driven cavity are controlled by two parameters; *i*) Reynolds number based on the lid motion velocity and the depth of the cavity; *ii*) the aspect ratio of cavity. These flow structures will change due to an inserted square or circular cylinder within the cavity. Understanding the influence of the inserted cylinder on the flow structures is of fundamental importance in engineering applications like heat exchangers and electronic coolers.

Oztop et al.[1] and Khanafer and Aithal[2] numerically investigated mixed convection and heat transfer in a steady lid-driven square cavity containing a circular cylinder by using a finite volume method and a finite element formulation, respectively. They found that for the forced convection flow an increase in the cylinder's size leads to the primary vortex breaking up into two vortices, and various locations of the cylinder result in the movement of the vortex cores. Moreover, a large gap between isotherms which affects the heat transfer was present due to strong flow circulation (i.e. the vortex formed in the cavity).

The lid-driven cavity flow with multiple embedded obstacles were also investigated and applied to test the accuracy of some numerical methods, e.g. the immersed boundary method by Su et al.[3] and the immersed interface method by Ito et al.[4] due to its low computational cost. Moreover, in the absence of the lid motion, many investigations were conducted for the natural convection (dominated by the temperature gradient) in a cavity containing obstacles with different locations and geometries (see e.g. [5, 6, 7]).

A thorough investigation of the vortex structures for steady lid-driven cavity flow containing a cylinder has, to the limit of author's knowledge, not been conducted in detail for purely forced convection flow. The present paper provides a detailed investigation of vortex structures in a two-dimensional steady lid-driven cavity of depth to width ratio 1/3 with an embedded circular cylinder with a dimensionless radius of 0.2 (i.e. the ratio between the cylinder radius and the cavity depth). Three different Reynolds numbers (100, 500 and 1000) based on the depth of the cavity and three different locations of the cylinder have been considered. A direct forcing immersed boundary method combined with the finite difference method proposed by e.g. Fadlun et al. [8] and improved by Peller et al.[9] is applied due to its easy meshing and efficiency of solving the Navier-Stokes equations in Cartesian grids.

2. Problem formation and numerical method

The flow with a constant density ρ and kinematic viscosity ν is governed by the two-dimensional Navier-Stokes equations described as follows:

$$\frac{\partial u_i}{\partial x_i} = 0 \tag{1}$$

$$\frac{\partial u_i}{\partial t} + \frac{\partial u_i u_j}{\partial x_j} = -\frac{\partial p}{\partial x_i} + \frac{1}{Re}\frac{\partial^2 u_i}{\partial x_j \partial x_j} \tag{2}$$

where the Einstein notation using repeated indices is applied. Here $u_i = (u,v)$ and $x_i = (x, y)$ for $i = 1$ and 2, are the velocity and Cartesian coordinates, respectively, whilst t, p and $Re = UH/\nu$ denote the dimensionless time, dimensionless pressure and Reynolds number, respectively, where H is the depth of cavity and U is the lid motion velocity. The time scale, pressure scale and length scale is H/U, $0.5\rho U^2$ and H, respectively.

Equations (1) and (2) are solved using a semi-implicit second order scheme in conjunction with a projection method, where Adams-Bashforth and Crank-Nicolson are applied to the convective terms and diffusive terms, respectively. A second-order central difference scheme is applied on a staggered mesh arrangement.

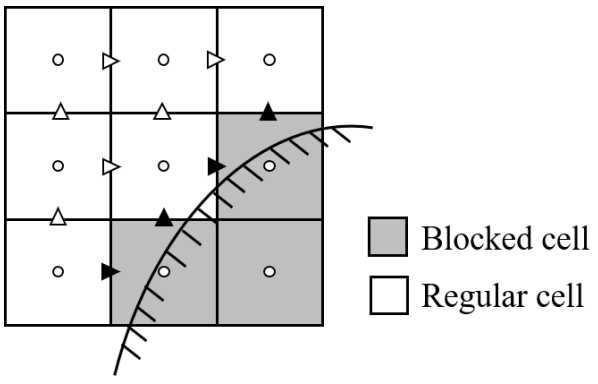

Figure 1. Definition of the blocked cell (grey square), the regular cell (white square), the active (white arrows) and inactive (black arrows) velocity points.

The immersed boundary method is based on a direct forcing approach combined with finite difference method. The relationship between the grid and the immersed boundary is shown in figure 1. A cell with the pressure point inside the solid is defined as a blocked cell while the rest cells inside the fluid are denoted by the regular cells. The velocity components at the connection face between the blocked and regular cells are set as inactive velocity points (▶ and

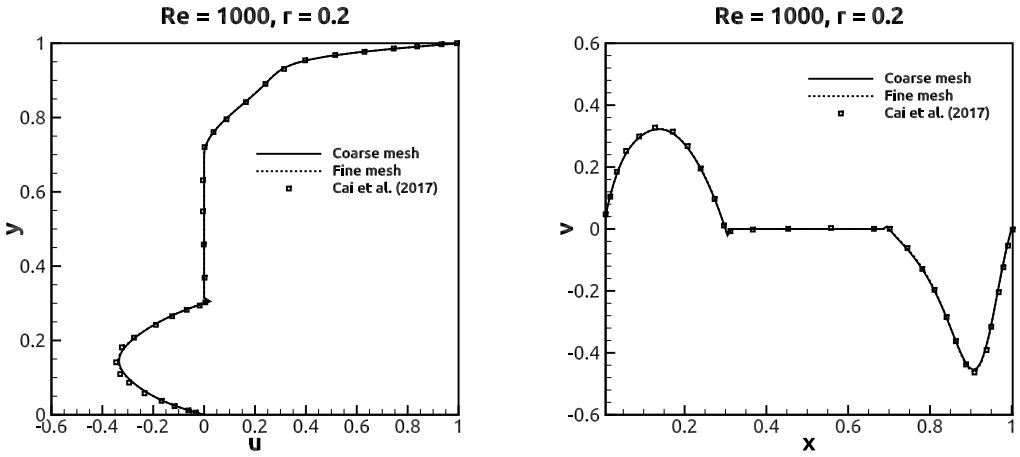

Figure 2. Comparison of the velocity profiles of the steady lid-driven cavity flow containing a centered cylinder of $r = 0.2$ for $Re = 1000$ obtained by the present method and by Cai et al.[11]: left image, distribution of velocity component u along $x = 0.5$; right image, distribution of velocity component v along $y = 0.5$.

▲), and those connecting two regular cells are considered as active velocity points (▷ and △). The inactive velocity points is updated by interpolation of its adjacent active velocity points. A linear interpolation applied in directions is given as follows

$$u_i = \frac{x_i - x_\Gamma}{x_{i+1} - x_\Gamma} u_{i+1} + \frac{x_{i+1} - x_i}{x_{i+1} - x_\Gamma} u_\Gamma, \quad i = 1, 2 \tag{3}$$

where u_Γ and x_Γ denote the velocity components and the position of the solid surface, respectively.

A weighting factor λ is introduced in Eq.(2) for the inactive velocity components which are interpolated from two directions[9, 10].

$$u_i = \lambda_x u_i^x + \lambda_y u_i^y \tag{4}$$

where the superscripts x and y denote the interpolation in x and y-directions, respectively. Moreover, a Neumann condition is applied for the pressure correction at the inactive velocity points.

3. Results and discussion

3.1. Verification against previous numerical results

A numerical simulation for flow in a steady lid-driven square cavity containing a centered circular cylinder has been conducted for $Re = 1000$. The velocity of the lid is given by $u = 1$, and no-slip conditions are imposed on the side and bottom walls as well as the cylinder. The dimensionless cylinder radius r equals to 0.2 ($= r'/H$). Two grid resolutions of 100×100 and 200×200 uniform cells are considered for the grid convergence test. Figure 2 shows the velocity profiles for u (left) and v (right) along $x = 0.5$ and $y = 0.5$, respectively. Previous numerical results obtained by Cai et al.[11] using an immersed boundary method which takes the body force as a Lagrange multiplier were included for comparison. A good agreement is obtained using both the coarse and fine meshes. It appears that the coarse mesh is sufficient to obtain the grid independent results.

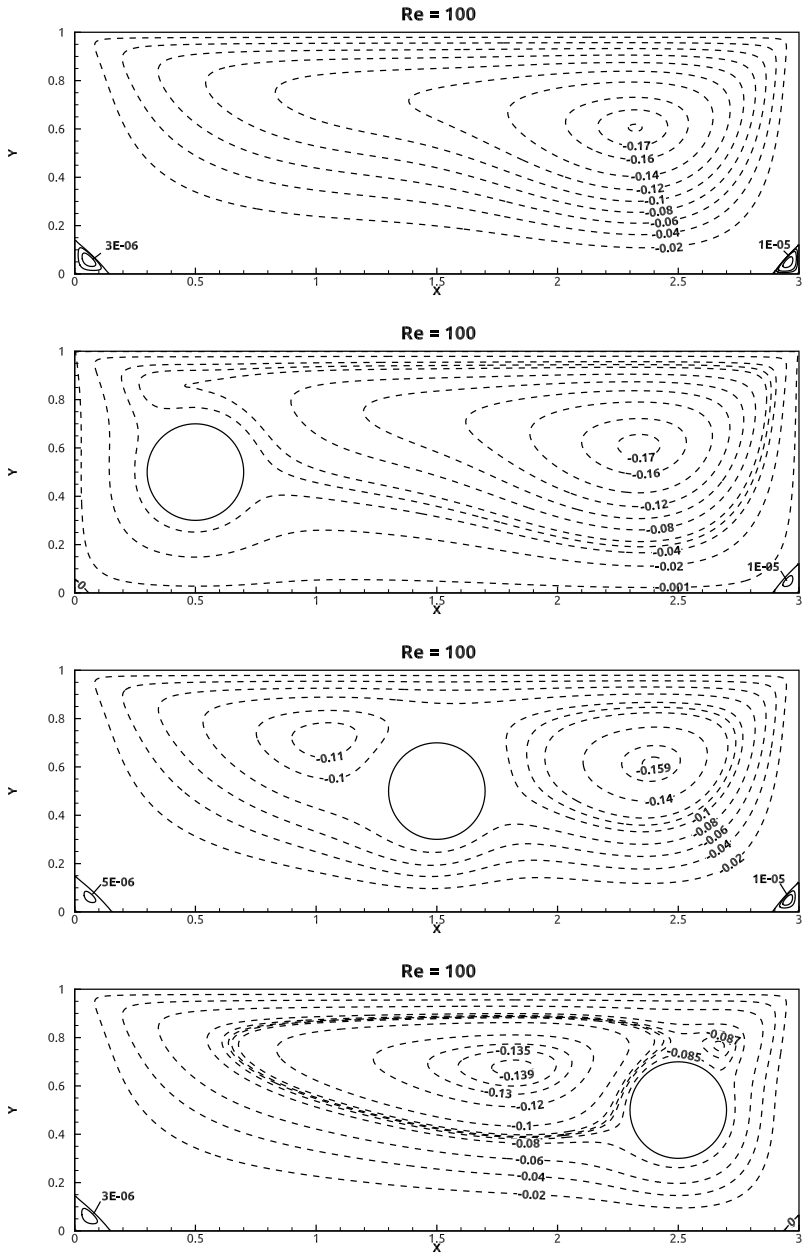

Figure 3. Streamfunctions within a steady lid-driven cavity of AR = 1/3 with and without a circular cylinder for Re = 100. The cylinder is positioned at (x, y) = (0.5, 0.5), (1.5, 0.5) and (2.5, 0.5).

3.2. Flow in a steady lid-driven rectangular cavity containing a circular cylinder

Predictions for flow in a steady lid-driven rectangular cavity containing a circular cylinder are presented for Re = 100, 500 and 1000 in this section. The depth to width ratios (AR) of the cavity is 1/3, and three different locations of the cylinder with r = 0.2 are considered to investigate their effects on flow structures. Moreover, the steady lid-driven cavity flows at respective Re are predicted for comparison purpose.

Figure 3 shows the streamfunctions within a steady lid-driven cavity of $AR = 1/3$ containing

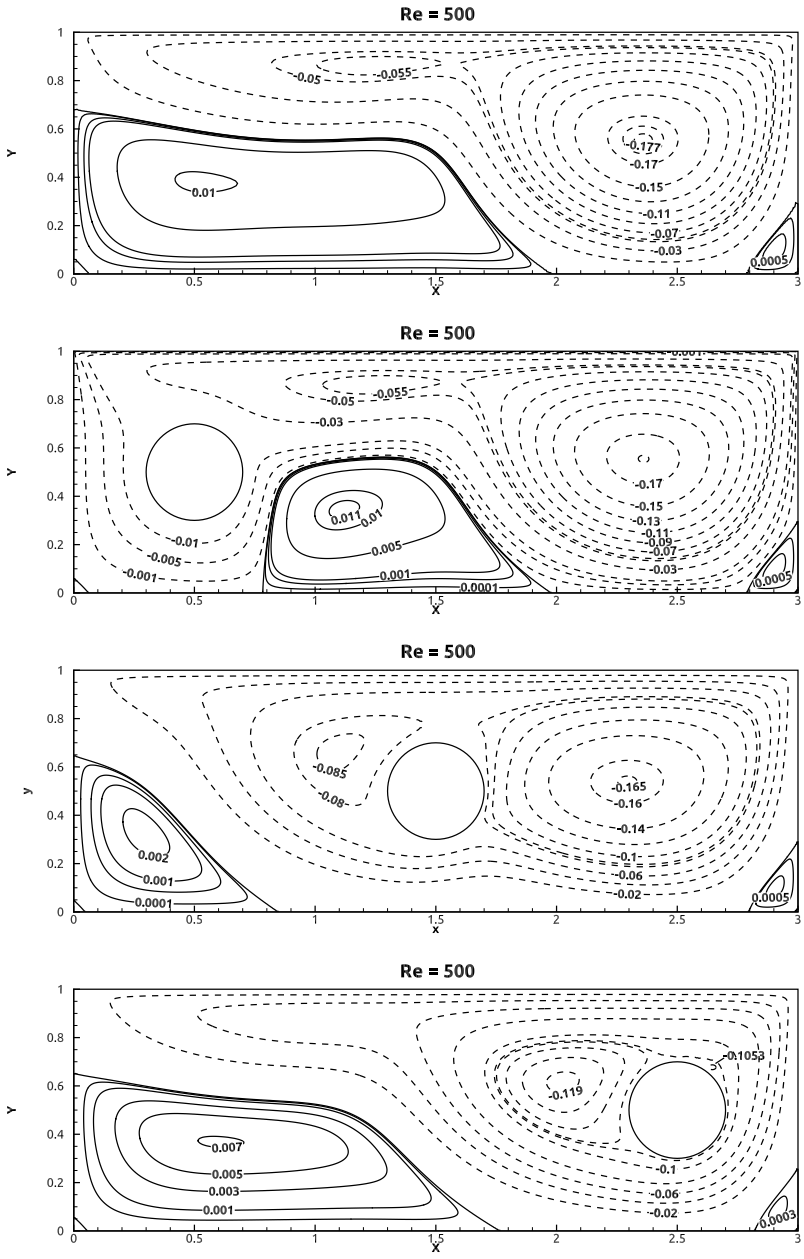

Figure 4. Streamfunctions within a steady lid-driven cavity of AR = 1/3 with and without a circular cylinder for Re = 500. The cylinder is positioned at $(x, y) = (0.5, 0.5)$, (1.5, 0.5) and (2.5, 0.5).

a circular cylinder for $Re = 100$. The cylinder is located at $(x, y) = (0.5, 0.5)$, (1.5, 0.5) and (2.5, 0.5). The cavity without the cylinder contains a clockwise primary vortex and two small anti-clockwise bottom corner vortices. These vortex structures qualitatively remain for the cylinder positioned at (0.5, 0.5) but with a slightly weaker primary vortex core and the nearly vanishing bottom left corner vortex. The bottom right corner vortex are weakly affected since it is far away from the cylinder. As the cylinder is positioned at (1.5, 0.5), the primary vortex present in the cavity without a cylinder appears to break into two clockwise vortices due to the presence of

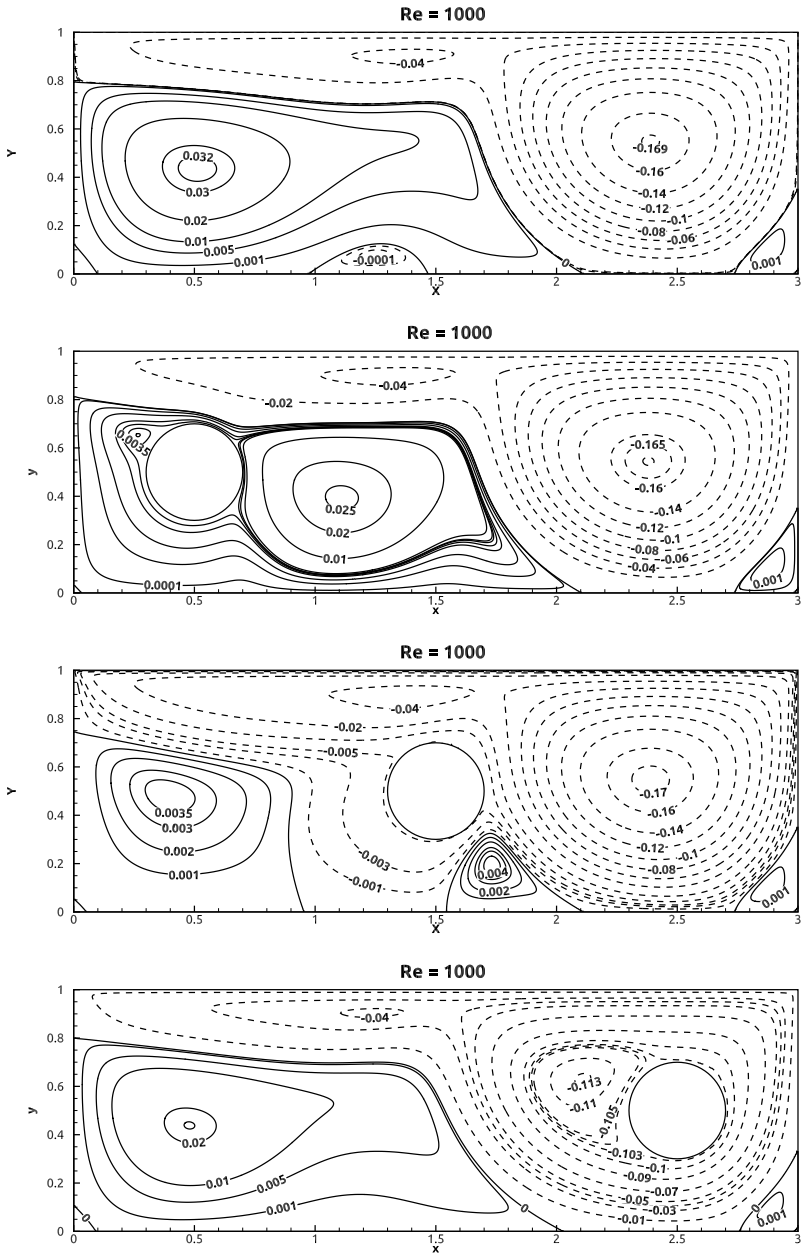

Figure 5. Streamfunctions within a steady lid-driven cavity of AR = 1/3 with and without a circular cylinder for Re = 1000. The cylinder is positioned at (x, y) = (0.5, 0.5), (1.5, 0.5) and (2.5, 0.5).

the cylinder at the right side of which the flow driven by the lid rolls down. Similar qualitatively vortex structures were previously investigated by Young et al.[12] for creeping flow within a steady lid-driven rectangular cavity with a centered cylinder. They found two equal clockwise vortices attached to the upper left and right side of the cylinder, respectively. In present cases, the non-linear effect from the convective terms attributes to the asymmetry of the attached vortices where the left one is smaller and weaker than the right one. As the cylinder is shifted to (2.5, 0.5), a decrease in space between the cylinder and the right wall suppresses the growth

of the right vortex, causing the left vortex becoming larger than the right one. This behavior qualitatively remains the same for $Re = 500$ as the cylinder moves rightwards from (1.5, 0.5) to (2.5, 0.5) shown in figure 4.

Figure 4 shows the streamfunctions for the same geometry shown in figure 3 but for $Re = 500$. In the cavity without the cylinder, a new clockwise vortex is formed beneath the lid, and flow separation occurs at $x = 2$, forming a larger bottom corner than that for $Re = 100$ (figure 3). As the cylinder is inserted at (0.5, 0.5), flow separation remains at $x = 2$ while the presence of the cylinder leads to the flow rolling down at the lower right side of the cylinder and reattaching the bottom wall, thus forming a large bottom vortex. For the cylinder located at (1.5, 0.5) and (2.5, 0.5), the clockwise vortex beneath the lid disappears, forming qualitatively similar vortex structures present for $Re = 100$ (figure 3) but with stronger vortex cores. Moreover, the attached vortices for $Re = 100$ (figure 3) is larger than those for 500 (figure 4) with the cylinder located at (2.5, 0.5). It appears that an increase in Re leads to a higher flow velocity around the cylinder, thus impeding the growth of the attached vortices.

Figure 5 shows the streamfunctions for the same geometry shown in figure 3 but for $Re = 1000$. In the cavity without the cylinder, an increase in Re forms a larger bottom left corner vortex and a small clockwise bottom vortex. This small bottom vortex disappears as the cylinder is inserted in the cavity. For the cylinder positioned at (0.5, 0.5), the cylinder is surrounded by a stronger anti-clockwise flow circulation due to a larger Re, such that the flow rolls down at the right side of the cylinder and up at the upper left side of the cylinder, forming two anti-clockwise attached vortices. The right one is much larger than the left one. As the cylinder is positioned at (1.5, 0.5), the bottom left corner vortex present in the cavity without the cylinder appears to break up into a large bottom left corner vortex and a bottom vortex. As the cylinder moves to (2.5, 0.5), the primary vortex in the cavity without the cylinder disappears (due to a higher Re) while the flow rolls up at the upper left side of the cylinder, forming the left attached vortex.

4. Summary and conclusion

The present paper provides a detailed investigation for flow in a steady lid-driven cavity of depth to width aspect ratio 1/3 containing a circular cylinder with a radius equals to 0.2. Three different Reynolds numbers and three different locations are considered. For a lower Reynolds number ($Re = 100$), the cylinder causes the flow rolling up and down, forming two clockwise vortices. As the cylinder moves rightwards, the left one grows while the right one decays. For a moderate Reynolds number ($Re = 500$), a large bottom vortex is formed for cylinder located near the left wall, and it disappears as the cylinder moves rightwards. For the largest Reynolds number ($Re = 1000$), two attached anti-clockwise vortices are formed around the cylinder located near the left wall. As the cylinder moves gradually closer the left wall, a large bottom vortex is formed and disappears together with the clockwise vortex to the right side of the cylinder.

Acknowledgement

We gratefully acknowledge the support for this research from the Department of Marine Technology, Norwegian University of Science and Technology and the China Scholarship Council (Grant no. 201506680058).

References

[1] Oztop H F, Zhao Z and Yu B 2009 *International Journal of Heat and Fluid Flow* **30** 886–901
[2] Khanafer K and Aithal S 2013 *International Journal of Heat and Mass Transfer* **66** 200–209
[3] Su S W, Lai M C and Lin C A 2007 *Computers & Fluids* **36** 313–324
[4] Ito K, Lai M C and Li Z 2009 *Journal of Computational Physics* **228** 2616–2628
[5] Ghaddar N K 1992 *International journal of Heat and Mass Transfer* **35** 2327–2334
[6] De A K and Dalal A 2006 *International Journal of Heat and Mass Transfer* **49** 4608–4623
[7] Lee J, Ha M and Yoon H 2010 *International Journal of Heat and Mass Transfer* **53** 5905–5919

[8] Fadlun E, Verzicco R, Orlandi P and Mohd-Yusof J 2000 *Journal of Computational Physics* **161** 35–60
[9] Peller N, Duc A L, Tremblay F and Manhart M 2006 *International Journal for Numerical Methods in Fluids* **52** 1175–1193
[10] Berthelsen P A and Faltinsen O M 2008 *Journal of Computational Physics* **227** 4354–4397
[11] Cai S G, Ouahsine A, Favier J and Hoarau Y 2017 *International Journal for Numerical Methods in Fluids* **85** 288–323
[12] Young D, Chen C, Fan C, Murugesan K and Tsai C 2005 *European Journal of Mechanics-B/Fluids* **24** 703–716